FUSE Observations of Molecular Hydrogen in Translucent Interstellar Clouds: II. The Line of Sight Toward HD 110432

Brian L. Rachford[1], Theodore P. Snow[1], Jason Tumlinson[1], J. Michael Shull[1], E. Roueff[2], M. Andre[3], J.-M. Desert[4], R. Ferlet[4], A. Vidal-Madjar[4], and Donald G. York[5],

ABSTRACT

We report the second study from the *FUSE* survey of molecular hydrogen in translucent clouds, for the line of sight toward HD 110432. This star lies beyond the Coalsack dark nebula, and with $E(B-V) = 0.40$, and $A_V = 1.32$ this line of sight bridges the gap between less extinguished diffuse cloud lines of sight with $A_V \sim 1$, such as ζ Oph, and the translucent clouds with $A_V \gtrsim 2$ such as HD 73882. Through profile fitting and a curve-of-growth analysis, we have derived rotational populations for H_2 for $J = 0$–7. The line of sight has a total molecular hydrogen column density, log N(H_2) = 20.68 $\pm$ 0.05 cm^{-2}, nearly identical to that toward ζ Oph, but a factor of three less than HD 73882. The ratio of N(J=1) to N(J=0) yields a kinetic temperature $T_{kin} = 63 \pm 7$ K, similar to other lines of sight with $A_V \gtrsim 1$. The high-J lines show considerable excitation above this temperature. However, the high-J lines cannot be well-fit to a single excitation temperature, and the even-J lines of para-hydrogen appear slightly enhanced relative to the odd-J lines of ortho-hydrogen. The high-J excitation is similar to that toward ζ Oph, but much smaller than that toward HD 73882. Chemical modeling indicates that the physical conditions in the cloud(s) are very similar to those in the cloud(s) toward ζ Oph. An analysis of *IUE* spectra of the Lyman-α line gives log N(H I) = 20.85 $\pm$ 0.15 cm^{-2}. Combined with N(H_2), we derive a hydrogen molecular fraction, $f_{H2} = 0.58 \pm 0.12$, statistically identical to that found for the lines of sight toward ζ Oph and HD 73882. From the *FUSE* data, and a curve-of-growth analysis using the same component structure as H_2 we find log N(HD) = $15.2^{+0.7}_{-0.4}$ cm^{-2}, between the values found for ζ Oph and HD 73882. Profile fitting suggests smaller b-values for HD than for H_2 and a value log N(HD) = $16.0^{+0.2}_{-0.3}$ cm^{-2}. From *FUSE* and *IUE* data we derive log N(CO) $\approx$ 14.3 cm^{-2} assuming the same component structure as CH, or log N(CO) $\approx$ 14.8 cm^{-2} if all the observed CO is co-spatial with the strongest CH component. From the combined measurements of hydrogen and carbon-containing molecules,

[1]CASA, University of Colorado, 389 UCB, Boulder, CO 80309

[2]DAEC, Observatoire de Meudon, F-92195 Meudon, France

[3]Department of Physics and Astronomy, The Johns Hopkins University, 3400 N. Charles St., Baltimore, MD 21218

[4]Institut d'Astrophysique de Paris, CNRS, 98bis, Blvd. Arago, F-75014 Paris, France

[5]Astronomy and Astrophysics Center, University of Chicago, 5640 S. Ellis Ave., Chicago, IL 60637

the line of sight toward HD 110432 appears quite similar to the diffuse cloud line of sight toward ζ Oph, and quite dissimilar to the translucent cloud line of sight toward HD 73882. Upcoming *FUSE* observations will further explore the transition between diffuse and translucent clouds.

Subject headings: ISM: abundances — ISM: clouds — ISM: lines and bands — ISM: molecules — stars: individual (HD 110432) — ultraviolet: ISM

1. Introduction

The wavelength coverage and sensitivity of the *Far-Ultraviolet Spectroscopic Explorer* (*FUSE*) opens new windows for the study of interstellar material toward fainter stars with more extinction than have been studied previously in the far-UV (Moos et al. 2000). In particular, this wavelength range gives access to the numerous transitions of molecular hydrogen (H_2) and deuterated molecular hydrogen (HD) below 1130 Å that cannot be studied with other existing instruments. In addition, the sensitivity is much greater than previous instruments capable of observations at similar wavelengths such as *Copernicus* and *ORFEUS*.

In Snow et al. (2000; hereafter Paper I) we presented an analysis of H_2 for HD 73882, the first translucent cloud line of sight observed with *FUSE*. For this line of sight, with $A_V = 2.44$, we found an H_2 total column density, log N(H_2) = 21.08, about 3 times as great as that found for lines of sight with $A_V \sim 1$. The hydrogen molecular fraction, f_{H2}, for HD 73882 was comparable to the largest values found for diffuse cloud lines of sight. In a companion paper, Ferlet et al. (2000) presented an analysis of HD for the same line of sight, finding log N(HD) = 16.1, but with large uncertainty. Again, this value is considerably larger than that found for ζ Oph-like lines of sight.

The *FUSE* translucent cloud survey program involves 36 lines of sight with A_V = 1–5, and is described in more detail in Paper I. In the current paper we present our second analysis of H_2 and HD from this program, for the line of sight toward HD 110432. With $A_V = 1.32$, this line of sight represents the transition between diffuse clouds like those along the line of sight toward ζ Oph, and the translucent cloud lines of sight with larger extinction such as HD 73882. Given that some of the material that contributes to the extinction may not be co-spatial with the molecular gas, a larger A_V does not guarantee that the H_2 and HD measurements are sampling a different environment. Good-quality data exist for HD 110432 for the entire wavelength range covered by *FUSE* (912–1187 Å), and this is the most complete study to date of H_2 for a line of sight with significant reddening.

In § 2 we discuss previous measurements along this line of sight. In § 3 we present a detailed description of our analysis procedures. In § 4, 5, and 6 we present, discuss, and summarize our results, respectively.

2. The line of sight toward HD 110432

HD 110432 lies beyond the southern Coalsack at a distance of 300 ± 50 pc (*Hipparcos*; ESA 1997). At $V = 5.24$, HD 110432 is one of the brightest stars lying behind substantial interstellar material with substantial UV flux not observed by *Copernicus*.

2.1. Spatial distribution of IS material along the line of sight

While considering the material between us and the star, we must carefully consider the star itself. HD 110432 is a Be star with a somewhat uncertain spectral type. Literature values derived from photometry and spectroscopy range in subtype from O9 to B2, and in luminosity class from III to V. The ionized circumstellar material that gives rise to the emission-line behavior also contaminates determinations of interstellar color excess and extinction, fundamental parameters for the comparison of lines of sight.

Codina et al. (1984) derived $E(B-V) = 0.40$ and a spectral type of B0.5 IIIe from *IUE* spectra. However, they also derive a distance of 430 ± 60 pc, somewhat larger than the *Hipparcos* distance. Seidensticker (1989) performed a comprehensive analysis of stars in the Coalsack region, deriving $E(B-V) = 0.52$ for HD 110432, a photometric spectral type of O9 Ve, and a distance of 400 ± 120 pc. However, the color excess was anomalously high for its distance relative to other stars in the immediate region. Most interestingly, Dachs, Engels, & Kiehling (1988) derived $E(B-V) = 0.49$, but attributed 0.09 magnitudes of this color excess to the circumstellar material. The remaining color excess is identical to that of Codina et al. (1984) which was unaffected by the circumstellar material at such short wavelengths, and should reliably characterize the material producing the interstellar absorption lines. At the same time the *total* color excess agrees well with the value from Seidensticker (1989), whose method would have included the circumstellar component. We thus adopt $E(B-V) = 0.40$ to represent the interstellar material containing the H_2 and HD.

The UV photometric extinction curve for HD 110432 was classified as "peculiar" by Meyer & Savage (1981). The normalized extinction, $E(\lambda-V)/E(B-V)$, for this line of sight is much smaller than the Galactic average, particularly for the shortest wavelength measurements at 1550 and 1800 Å. This result suggests a much above-average value of total-to-selective extinction, R_V. However, as we have already noted, the Be nature of this star must be considered. Meyer & Savage (1981) used $E(B-V) = 0.51$, but with our preferred interstellar value of $E(B-V) = 0.40$, the interstellar extinction curve appears much closer to the Galactic average. Part of this correction may be offset by adjustment of V in the calculation of $E(\lambda-V)$, but even this effect is fractionally smaller for a fixed ΔV at the shorter wavelengths due to the larger color excesses at those wavelengths.

The wavelength of maximum polarization, $\lambda_{\max}$, has been shown to be linearly correlated with R_V (Serkowski, Mathewson, & Ford 1975). In addition, while the observed polarization towards Be stars may be influenced by local polarization of circumstellar material, this effect is small in the

face of substantial interstellar material, and should not affect $\lambda_{\rm max}$ (Whittet & van Breda 1978). Serkowski et al. (1975) found $\lambda_{\rm max} = 0.59$ μm, corresponding to $R_V = 3.3$, slightly larger than the Galactic average of 3.1. Combined with our adopted color excess, we obtain $A_V = 1.32$, consistent with the value from Seidensticker (1989) minus the effects of the circumstellar material.

The absorption along this line of sight is dominated by the Coalsack, a prominent dark nebula centered near the same RA and Dec as HD 110432. The distance to the nebula has been derived by photometric analysis of stars in the field by many authors. The value of 174 ± 14 pc from the early photographic study of Rodgers (1960) has held up well. Franco (1989) derived 180 ± 26 pc from photoelectric data. Seidensticker & Schmidt-Kaler (1989) considered more stars and found evidence for two sub-clouds at distances of 188 ± 4 and 243 ± 14 pc with the latter cloud providing somewhat greater extinction than the former. The morphology of the extinction map agrees well with the CO emission map of Nyman et al. (1989). No matter what the true distribution of material may be, at 300 pc HD 110432 lies behind all of this material with very little extinction between the Coalsack and the star. In addition, foreground material represents a small fraction of total absorption along the line of sight ($A_V \sim 0.1$ mag; Seidensticker & Schmidt-Kaler 1989).

2.2. Cloud velocity structure

An accurate assessment of the H_2 velocity structure is crucial for the interpretation of the high-J lines, and the resolution of the *FUSE* spectra is generally insufficient for this purpose. Since individual components typically have velocity spread parameters, $b \sim 1$–2 km s^{-1}, resolution of comparable magnitude is preferred. Fortunately, HD 110432 has been observed at ultra high resolution ($\Delta v = 0.3$ km s^{-1}), at optical wavelengths (Crawford 1995). These observations provided velocity structures for CH, CH^+, Ca II, and K I. Of most relevance to H_2 are CH and K I.

The CH observations reveal a simple velocity structure with just two components separated by 4.0 km s^{-1}. The K I profile is somewhat more complex, with five components, dominated by two strong components separated by 1.3 km s^{-1}. The combined profile of the two closely-spaced strong K I components plus one of the weak components rather closely matches the overall shape of the strong CH component. Further, the profile of the remaining two weak K I components spans the same velocity range as the weaker CH component, albeit this latter component did not appear to be double. Since the overall line profiles are generally similar, the "effective" b-values for the two profiles are also similar, 2.4 km s^{-1} for CH and 2.1 km s^{-1} for K I. Given the low molecular hydrogen kinetic temperature we derive (63 K; § 4), the velocity dispersion is dominated by turbulent motion and not thermal motion. Thus, scaling the CH b-values to H_2 according to mass only increases the effective b-values by about 10%, and these scaled values were used to generate the adopted component structure given in Table 1. While we use the CH structure to model the H_2 structure, the K I structure would give similar results. In § 4 we describe two tests which support this choice of velocity structure for H_2.

Other species have been observed in absorption at resolutions of $\Delta v \sim 3$ km s^{-1}, and Table 2 gives a summary of the column densities of previously observed molecules and atoms. As van Dishoeck & Black (1989) first pointed out, the column densities of molecules such as C_2, CH, and CN are more typical of diffuse cloud lines of sight such as ζ Oph, than translucent clouds. The value of N(CO) from Codina et al. (1984) is very uncertain, and in § 5 we derive a more precise value based on additional *IUE* spectra unavailable to those authors, and revised oscillator strengths.

Millimeter-wave CO measurements with a $43''$ beam show little if any emission at the velocities of the previously mentioned absorption features (Gredel et al. 1994), but do show a strong component at $v_{\rm LSR} = 5.1$ km s^{-1} ($v_{\rm helio} = -2.5$ km s^{-1}), about 5 km s^{-1} blue-shifted from the bluest absorption components. As pointed out by Crawford (1991), the absorption line data support the conclusion of Nyman et al. (1989) that the CO emission at this velocity near HD 110432 represents background material.

3. *FUSE* Observations and Data Analysis

HD 110432 was observed by *FUSE* on 2000 Apr 4–5 for a total of 3631 seconds spread across 5 short integrations. Due to the relatively large UV-flux, the data were recorded in spectral image mode (Moos et al. 2000). In this mode, integration times are kept short to prevent detector and spacecraft motion from degrading the spectral resolution. Excellent data were recorded on all 8 detector segments, with stellar signal recorded essentially down to the Lyman limit as Figure 1 indicates. The data were processed with version 1.6.9 of the CALFUSE pipeline, but we have used a later, improved version of the wavelength solution. We have co-added the 5 integrations for each segment, propagating the pixel-by-pixel uncertainties through the co-additions. Given the differences in the wavelength scales and line-spread functions of the different detector segments, we have not combined data from different segments even though the wavelength ranges overlap. We emphasize that while the spectrum depicted in Figure 1 was formed by combining all detector segments, this spectrum is primarily useful for display purposes and is not suitable for precise measurements.

With the full wavelength coverage of *FUSE* available for this target, a wealth of information on H_2 is available. The spectrum is dominated by the heavily damped and blended $J = 0$ and $J = 1$ lines from the Lyman series (B–X) vibrational bands from (0,0) through (18,0), and the Werner series (C–X) vibrational bands from (0,0) through (4,0). At shorter wavelengths, the strongly damped Lyman series H I lines become progressively more important. The H_2 lines for $J = 2$ also show damping wings, while the progressively weaker $J = 3$ through $J = 7$ line profiles are dominated by the apparently Gaussian line spread function. Given the various H_2 line profiles encountered, we use multiple techniques to derive column densities, and we describe those techniques in detail as they will be used in the analysis of all additional targets in this program.

At total H_2 column densities greater than $\sim 10^{20}$ cm^{-2} the overlapping profiles from adjacent

bands conspire to create a spectrum where the true continuum level is never reached. Figure 2 shows a normalized model spectrum for H_2 corresponding to the $J = 0$ through $J = 5$ column densities we derive for HD 110432. The effect of the overlapping bands is smallest for the longest wavelength vibrational bands due to the combination of having fewer contributing bands on the red side, and smaller oscillator strengths for these bands. Shortward of 1010 Å, the effect is magnified by overlapping Lyman and Werner bands. Most of our program stars have even larger column densities with correspondingly greater effect. An important consideration then is that the continuum can not be located *a priori*.

Thus, to determine the column densities for $J = 0$ and $J = 1$, we must perform profile fits to as many vibrational bands as is practical, with the continuum being a fit parameter. However, there are several complicating factors. First, the saturated cores of $J = 0$ and $J = 1$ blends provide no leverage in the continuum determination. Second, the H_2 lines with $J \geq 2$, as well as lines from other species must be included in the fit. Third, some H_2 profiles are contaminated by stellar lines, as well as idiosyncrasies in the large-scale response of the detectors. Fourth, the effects of $J = 0$ and $J = 1$ line wings from adjacent bands cannot be ignored. Finally, blends between the Lyman and Werner series H_2 lines, and blends of H_2 and H I lines limit the number of H_2 bands that can be fitted with the highest accuracy.

To overcome the first factor, we must include a significant wavelength range in the fits, typically about 10 Å per band. For the second factor, we include all H_2 lines up to $J = 5$, as well as identifiable lines of other atomic and molecular species. The weaker lines carry little weight in the overall fits, and they are not always modeled as accurately as if they were treated individually, but do allow for accurate continuum placement. To alleviate the other continuum problems, we removed the obvious stellar lines by dividing by an appropriate Gaussian profile. Also, we only fit one band at a time such that we can model the local continuum with a low-order polynomial. To overcome the fourth factor, we explicitly include the effects of all the $J = 0$ and $J = 1$ lines within 30 Å of the region we are fitting. As for the selection of H_2 bands to fit, the Lyman bands from (0,0) through (4,0) are clean of Werner bands and H I lines. Each of these bands occurs in 2, 3, or 4 detector segments.

In the particular case of HD 110432, we were unable to obtain good fits for the (0,0) band, presumably due to stellar contamination in the lower portions of the wings, or at the narrow "bump" between the R(0) and R(1) lines. Without resorting to unverifiable guesses as to the nature of contamination, or a full non-LTE modeling of the stellar spectrum, we could not use this band for this line of sight. However, in other program stars with different (generally earlier) spectral types, this effect may not be important. Even without the (0,0) band, we still have a total of 13 profiles from which to derive the low-J column densities. Figure 3 shows a sample fit of the (2,0) band covering the 1072–1082 Å region.

For $J \geq 2$, the lines are weak enough that one can measure individual equivalent widths by fitting Gaussian profiles to each line, or resolved blends of lines. These measurements are relative

to the observed background level; i.e. the J=0–1 line wings. We were able to measure at least one individual H_2 line of $J \geq 2$ from each Lyman-series vibrational band from (0,0) through (18,0), and from each Werner-series vibrational band from (0,0) through (4,0). In total, we obtained 249 equivalent width measurements for 99 H_2 transitions. In 22 cases, we were able to measure a transition in the maximum possible 4 detector segments, and for all but 15 transitions we measured the line in at least 2 segments, allowing us to check the data for self-consistency.

The lines of HD behave much like the high-J lines of H_2. Typically, the equivalent widths of the $J = 0$ lines of HD are similar to those of the $J = 4$ and $J = 5$ lines of H_2. The $J = 1$ lines of HD are considerably weaker, and conclusive detection of such lines in our *FUSE* spectra will generally be difficult. For HD 110432, we obtained 24 equivalent width measurements for 8 $J = 0$ lines, and none for $J = 1$.

We determine an error estimate for each line measurement based on the formal uncertainty of the Gaussian fit parameters, combined in quadrature with a formal estimate of the uncertainty in continuum placement. In combining measurements of the same line from different detector segments, we must be careful how we treat systematic differences. A simple weighted mean of the individual measurements will provide encouragingly small uncertainties when several measurements are combined, but if the actual values cover a large range, this reported uncertainty is not useful. However, the standard deviation is not useful considering the small number of measurements. The procedure we have adopted takes the largest of the three following numbers: one-half of the total range of measurements for a particular line (a proxy for the standard deviation), the error we derive from a weighted mean, and 10 per cent of the weighted mean itself. The latter limit provides a conservative estimate of any systematic errors that we may not have considered. There are six pairs of detector segments whose wavelength coverage overlap. In comparing equivalent widths for the same line in these pairs of segments, we find excellent agreement with an exact one-to-one relationship. The only possible exception is for the SiC 1A and SiC 1B segments where the strongest lines were consistently measured to be 10–15% stronger than in other segments. However, this only involves a half-dozen lines, mostly from $J = 2$ where we used profile fitting for the final column densities, as discussed below.

From the final equivalent width measurements, and the assumed velocity structure, we construct a multi-component curve of growth. Using the uncertainties of the individual lines, we perform a least-squares fit for each J to determine N(J) for H_2 and HD.

The $J = 2$ lines of H_2 represent a special case. They are strong enough to have noticeable damping wings, yet the surrounding continuum is frequently not clean enough to allow accurate fitting of those wings with an individual damped Voigt profile. The Gaussian profile fitting, used in the measurement of the weaker lines, underestimates the equivalent widths of the strongest $J = 2$ lines by as much as 10–15% for HD 110432, which corresponds to a 0.1–0.2 dex underestimate of the column density. However, the profiles of these damped lines are fitted well along with the $J = 0$ and $J = 1$ profiles, which gives us slightly better results than the curve of growth analysis for

this particular line of sight.

The confusion between the H_2 bands and the H I lines makes a determination of N(H I) somewhat difficult using *FUSE* data. However, this method may eventually produce accurate column densities, especially for cases where N(H I) >> N(H_2); i.e. where the hydrogen molecular fraction is small. In the case of HD 110432, we have used *IUE* spectra of Lyman-α to determine N(H I). We co-added all 13 available SWP spectra from the *IUE* archive to improve the S/N. We used the technique of Bohlin (1975) to determine the best column density by matching a pure damping profile to the observed line wings. The primary uncertainty in this method beyond the noise in the data is the presence of stellar lines in the wings of Lyman-α, particularly the blue wing. As we discuss in § 4, the actual component structure can only have a small effect on the derived N(H I).

4. Results

We begin with the results of the band-by-band profile fits. Table 3 summarizes these results. Fits of the same band in different detector segments show exceptional agreement. However, band-to-band differences exist. In all segments, the (3,0) band yields larger column densities for $J = 0$. The mean of the (3,0) values is about 0.15 dex larger than the mean from the other bands. The $J = 2$ column densities are also slightly larger than those from the other bands, but the $J = 1$ columns are not significantly larger. A visual inspection of the (3,0) band fits does not reveal an clear explanation for the differences, although one or more stellar lines may be the culprit. We have included these values in the final averages given in Tables 3 and 4 although it may be appropriate to exclude this band in future studies. The reported uncertainties for $J = 0$–2 are simply the sample standard deviation of the 13 individual values. If we exclude the (3,0) results, the uncertainty is cut in half for $J = 0$, while the average value decreases by 0.04 dex.

Figure 4 shows the 2-component curve of growth along with our averaged measurements of 99 H_2 transitions and 8 HD transitions. Since the uncertainties in N(J) for H_2 lines of $J \geq 3$ and the HD lines are affected by the shape of the curve of growth, we have given two-sided 1-σ error bars to these values in Table 4. For HD 110432, most of the error bars do not show much asymmetry. We emphasize that the uncertainties in these values of N(J) only apply to the assumption that we have a perfect description of the component structure. Changes in the component structure can produce changes in column densities when the lines lie on or near the flat portion of the curve of growth. For instance, if we had used the K I structure, our derived column densities for $J = 3$–6 would be increased by 0.10, 0.20, 0.25, and 0.10 dex, respectively. While these changes are modest, if we have seriously misjudged the H_2 velocity structure, the changes could be much greater.

With this point in mind, we performed two additional tests of the validity of our assumed velocity structure. First, given the H_2 equivalent width data, we fitted a single-component curve of growth, allowing both the column densities and the b-value to vary. The best-fit b-value, and in turn

the column densities, were consistent with the "effective" b-value and column densities of the two-component model. Second, we performed profile fits to several bands assuming a two-component structure with velocity separation given by the CH data, but allowing the b-values and relative strengths of the components to vary. Again, the derived component parameters were consistent with the CH structure. Both tests indicate that the changes in the column densities due to possible uncertainty in the component structure are not larger than the differences between the CH and K I structure indicated in the previous paragraph .

Our best curve-of-growth column density for $J = 2$ is 18.55, or 0.13 dex smaller than our profile fits, consistent with our previous discussion of the fitting of the $J = 2$ lines. The column density for $J = 7$ is based on only one very weak line. Also, N(J=6) is based on just 4 weak lines with very little spread in λf. The small observed uncertainty thus may not be reliable.

Our fit of the H I Lyman-α line gives log N(H I) = 20.85 ± 0.15 cm^{-2}. We note that if instead of assuming a pure damping profile, we use the CH velocity structure and scale the b-values according to mass, log N would be about 0.05 dex smaller. However, even a slight increase in the complexity of the H I component structure relative to CH could decrease this difference to near zero.

Given the H_2 column densities (particularly for $J = 0$–5), and the H I column density, we can explore the physical conditions of the absorbing gas. When combined with log N(H I) = 20.85 ± 0.15 cm^{-2}, our total H_2 column density of log N(H_2) = 20.68 ± 0.05 cm^{-2} gives a molecular fraction $f_{H2} = 0.58 \pm 0.11$; i.e. between one-half and two-thirds of the observed hydrogen atoms exist in H_2 molecules. At the relatively high densities assumed to exist in these H_2 cloud(s), the ratio of N(J=1) to N(J=0) is considered an indicator of the kinetic temperature of the gas, and we derive $T_{\rm kin} = 63 \pm 6$ K.

The excitation diagram in Figure 5 shows the enhanced populations for $J \geq 2$ relative to the kinetic temperature of the gas. This non-thermal excitation is usually interpreted as pumping by UV photons, followed by cascading transitions down through the various rotational states (Black & Dalgarno 1973). The high-J lines in many lines of sight can be fitted by a single excitation temperature, i.e. a straight line in the excitation plot (Spitzer & Cochran 1973). For HD 110432 such a fit for J = 2–5 seriously overestimates N(J=3), and in general the even-J lines (para-hydrogen) appear slightly enhanced relative to the odd-J lines (ortho-hydrogen). However, good linear relationships do appear for J = 1–3 and J = 3–5. For the former levels, we derive a temperature $T_{13} = 110 \pm 5$ K, and for the latter, we derive $T_{35} = 240 \pm 40$ K. An even less certain fit for J = 3–7 corresponds to T ≈ 350 K.

5. Discussion

Several lines of sight with $A_V \sim 1$ were observed with *Copernicus*, ζ Oph being the prototype. We will present a detailed comparison of all lines of sight with $A_V \gtrsim 1$, including more than a dozen of our *FUSE* translucent cloud program stars in a future work (B. L. Rachford et al. 2001, in

preparation). In the current paper, we will generally limit our comparisons to ζ Oph (Morton 1975; Savage et al. 1977), HD 73882 (Paper I), and HD 110432, with only brief references to the larger survey. Relevant data for these lines of sight appear in Table 5. The lines of sight have similar total-to-selective extinction ratios, but cover a range of more than a factor of 2 in color excess and thus visual extinction.

The kinetic temperatures of the three lines of sight are statistically identical. In addition, our preliminary survey of *FUSE* translucent cloud program stars indicates H_2 kinetic temperatures of $\sim$60 K are typical for such lines of sight. The ratio $N(H_2)/A_V$ lies within the range 3.5–5 $\times$ 10^{20} cm^{-2} mag^{-1} for all three lines of sight, and the molecular fractions are nearly identical as well. However, these latter two ratios do not hold up in the larger survey. In particular, we see a large range in f_{H2} with a possible upper limit near 0.7. If verified, this upper limit may provide important information on formation and destruction mechanisms at H_2 column densities near 10^{21} cm^{-2}.

The combination of line saturation and the relatively limited range of log $f\lambda$ produces a very uncertain curve-of-growth value of N(HD) that falls squarely between the values for ζ Oph on the low side, and HD 73882 on the high side. The HD/H_2 ratio of 3 $\times$ 10^{-6} falls well below the expected value of 2$\times$D/H that would be observed if HD represents the primary reservoir of deuterium. However, if HD occurs primarily in the cores of the clouds(s) along this line of sight, the H_2 component structure may not be appropriate. Fits of the HD lines assuming a 2-component model that allow the strengths and b-values to vary, support this view. The best fits yield log N(HD) = $16.0^{+0.2}_{-0.3}$ cm^{-2}, with b-values of 1.4 and 1.2 km s^{-1} for the blue and red components, respectively, and a much weaker blue component than for H_2. This result gives an overall HD/H_2 ratio slightly smaller than typical values of 2$\times$D/H. The HD/H_2 ratio for the red component would be $\sim$4 $\times$ 10^{-5}, quite similar to 2$\times$D/H. However, we emphasize that the uncertainty is about a factor of 2.

As depicted in Figure 6, the excitation of the high-J levels of H_2 is similar to, but slightly larger than that of ζ Oph; yet is much smaller than HD 73882. Two factors control this excitation, the UV interstellar radiation field (ISRF) and the number density.

HD 110432 itself is an early enough star to excite H_2, and with the two-cloud structure of the Coalsack proposed by Seidensticker (1989), the star lies 60 $\pm$ 50 pc beyond the cloud at $\sim$240 pc. The other cloud, at $\sim$190 pc, would then lie 110 $\pm$ 50 pc from the star. To estimate the effects of HD 110432 on the Coalsack, we have taken fluxes at 1000 Å from an appropriate Kurucz (1979) model for a B0.5 III star (T_{eff} = 25000 K, log g = 3.5, solar metallicity), a stellar radius of 15$R_\odot$, and then compared the resultant radiation field at various distances from the star to the average ISRF (Mathis, Mezger, & Panagia 1983). Assuming no dimunition of the stellar radiation field between the star and the cloud(s), we find that at about 40 pc from the star the stellar field is equal to the average ISRF[6]. We can then safely assume that HD 110432 does not contribute

[6]If HD 110432 is actually of spectral type B2 Ve, this distance drops to around 10-15 pc.

significantly to the radiation field of the cloud at 190 pc, but we cannot make the same assumption about the other cloud. Even if the material is more uniformly distributed between 180 and 250 pc, the same conclusion holds; the material more distant from Earth may be affected by the radiation field from HD 110432 while the material nearest to Earth is not.

We have searched the *Hipparcos* catalog for other O and B stars in the region. In Figure 7, we present distances and spectral types for stars within about 6 degrees of HD 110432. There are many stars much closer than the Coalsack, and many more beyond the nebula, but few at the appropriate distances to be exciting the cloud(s) along this line of sight. At 174 pc, HD 110737 (302.2,−1.8) may lie within the nearest portion of the Coalsack, and is just 6 pc from the line of sight to HD 110432. However, at spectral type B9.5, this star has many orders of magnitude less UV flux than HD 110432, and little power to excite H_2. Two early B stars, HD 103884 at (296.6,0.7) and HD 104841 at (297.6,−0.5), lie at the same distance from Earth as the Coalsack, but lie 20 pc from the line of sight, well outside the boundaries of the cloud(s). Given the uncertainties in the *Hipparcos* distances, the uncertainties in the precise structure of the Coalsack, and the weaker UV output as compared with HD 110432, these stars may not provide much enhancement to the overall radiation field. For comparison, the ISRF impinging on the cloud(s) containing H_2 along the line of sight to ζ Oph is thought to be no more than twice the average field (Federman et al. 1995).

Through observations of weak, rotationally excited C_2 lines, van Dishoeck & Black (1989) estimated the number density of the material toward HD 110432, and find an uncertain value of $n \lesssim 200$ cm^{-3}. A similar analysis for ζ Oph (van Dishoeck & Black 1986) gives an uncertain value $n \approx 200$ cm^{-3}.

We have taken advantage of the amount of observational knowledge to run chemical models of translucent clouds. The basic assumptions are described in Le Bourlot et al. (1993). The model solves the radiative transfer as well as the chemical molecular formation/destruction mechanisms of a cloud containing H, C, N, O, and S species and a metal, illuminated by the ISRF. The thermal balance can be solved in parallel to the chemical equilibrium. The original model, which was devoted to study the envelopes of molecular clouds, consists of a semi-infinite planar slab where the radiation field is impinging on one side of the cloud. The photodissociation of H_2 is taking place through absorption in the discrete ultraviolet Lyman and Werner band transitions followed by continuous fluorescence. The photodissociation probabilities and the basic molecular properties of the Lyman and Werner band systems are accurately known from previous experimental and theoretical studies (cf. Roueff et al. 1999; Abgrall, Roueff, & Drira 2000). Such a model is very similar to other models of so-called Photon Dominated Regions (PDR) (see Hollenbach & Tielens 1999 for a recent review). It has been recognized recently (Le Bourlot 2000) that ortho to para conversion of molecular hydrogen may occur on grains. Moreover, the grain temperature depends critically on the photoelectric effect, i.e. on the actual value of the radiation field impinging on the grains at a certain location in the cloud . The models presented here follow the prescription of Le Bourlot (2000) and take into account the effect of the size distribution of the grains in the formation of H_2 on the grains (Le Bourlot et al. 1995) as well as in the determination of their

charge following Bakes & Tielens (1994).

In order to apply the model to a diffuse cloud line of sight such as HD 110432, we have additionally introduced the deuterium chemistry and the detailed mechanisms implied in the formation and destruction of HD (Le Petit, Roueff, & Le Bourlot 2001; in preparation) and we consider the cloud as a finite slab of constant density submitted to the same radiation field on both sides. The elemental abundances are the mean interstellar values given by Savage and Sembach (1999). The cosmic ray ionization rate is chosen to be 5×10^{-17} s^{-1}, a mean value deduced from OH observations (Federman, Weber, & Lambert 1996).

We assign model parameters to reproduce several observational constraints; namely, the hydrogen molecular fraction, the temperature-sensitive H_2 column densities in $J = 0$ and $J = 1$, and the total visual extinction. The ratio between the total hydrogen column density and A_V we have derived, 1.26×10^{21} cm^{-2} mag^{-1}, is slightly smaller than average. The ISRF may be somewhat larger than the mean standard value taken from Draine (1978) but its actual value is not known. The peculiar character of the extinction curve in the ultraviolet is taken into account via the R_V value of 3.3.

Within the series of models we have run, we find that the two main constraints are fulfilled for a ratio of about 100 between the proton density n_H and the multiplicative factor G_0 of the ISRF in Draine's units. Indeed, the molecular fraction is directly proportional to n/G_0. However, this agreement is obtained *only* when the minimum radius of the grains is larger than about 10^{-6} cm. This fact should be compared with the peculiarity of the extinction curve: the larger than normal value of R_V implies a far UV extinction lower than the mean value, in agreement with the absence of very small grains. This cut-off in the grain size distribution has two major effects, one on the formation rate of H_2 and thus on the value of the molecular fraction, and the other on the temperature governing the ratio between the $J = 1$ and $J = 0$ column densities. Table 6 gives the results of some typical models.

The actual value of the ISRF is not known but should not be larger than a few; so a density of about 200 cm^{-3} and a radiation field of about twice the standard ISRF provides a reasonable compromise, in agreement with the density found from the study of the excitation of C_2. With these parameters, a column density of deuterated molecular hydrogen of 1.1×10^{16} cm^{-2} is obtained, in agreement with the observations.

In contrast, none of the models reproduces the column densities of the rotational levels of molecular hydrogen with $J \geq 2$ as shown in Table 7. This not surprising due to the simplified geometry assumed. However, we feel that we address here a more fundamental failure of the chemical model. Indeed, the presence of the CH^+ molecular ion can not be reproduced by any PDR model and another chemical component is needed. This puzzle has been addressed by the presence of shocks (Pineau des Forêts et al. 1986) or by the occurrence of dissipative structures due to interstellar turbulence (Falgarone, Pineau des Forêts, & Roueff 1995; Joulain et al. 1998). The presence of an intense far ultraviolet radiation field may also lead to an efficient formation

mechanism of CH^+ as suggested by Snow (1993). However, no obvious candidate for the production of intense ultraviolet radiation is available in the environment of HD 110432. Such a tiny component, whatever its origin, will enhance the populations of excited molecular hydrogen without modifying the populations of $J = 0$ and $J = 1$. Further modeling is beyond the scope of the present paper and will be performed subsequently. This modeling may also reveal the significance, if any, of the slightly enhanced column densities of para-hydrogen relative to ortho-hydrogen.

For comparison, it appears that the density in the clouds toward HD 73882 is larger than for the lines of sight toward ζ Oph and HD 110432. An analysis of C_2 gives $n = 350^{+300}_{-100}$ cm^{-3} (Gredel, van Dishoeck, & Black 1993). In addition, the column densities of $J = 4$ and $J = 5$ are the largest yet observed for any diffuse or translucent line of sight. This may suggest a very strong UV field, a distinct possibility considering that HD 73882 has a spectral type of O8.5, even earlier than ζ Oph. As noted above, the current models are unable to reproduce the observed high-J excitation, and thus an interpretation of the extreme excitation seen toward HD 73882 will require further work.

The column densities of carbon-containing molecules along the line of sight toward HD 110432, such as CH, CH^+, and C_2, more closely match those of diffuse clouds rather than translucent clouds. However, the CO column density is rather poorly known and represents most of the carbon locked up in diatomic molecules. The millimeter wave observations of Gredel et al. (1994) reveal little if any CO emission at the velocities of the absorption lines of CH, etc. Codina et al. (1984) observed several of the CO absorption bands from the A–X series with *IUE* and derived log N(CO) = 14.60 cm^{-2} from a curve-of-growth analysis. This value was quite uncertain and depended on the then poorly-known velocity structure, and there have been subsequent revisions in the oscillator strengths for these bands.

In principle, N(CO) can be determined from *FUSE* data. Easily visible CO bands within the *FUSE* wavelength range include B–X (0,0) at 1150 Å, C–X (0,0) at 1088 Å, and E–X (0,0) at 1076 Å. The C–X (1,0) band at 1063 Å , E–X (1,0) band at 1052 Å, and F–X (0,0) band at 1003 Å have f-values large enough to be visible, but are lost in or near the cores of strong H_2 $J = 0$ and $J = 1$ lines.

The C–X (0,0) band is contaminated by interstellar atomic lines (Cl I λ1088.06 and others). Several weak lines lie slightly blueward and redward of the B–X (0,0) band but reasonable fits can be obtained in HD 110432. In the spectrum of HD 110432, the E–X (0,0) band lies in the blue wing of the $J = 0$ line of the Lyman (2,0) band of H_2, but is clean of narrow lines from other species. However, in lines of sight with much larger H_2 column densities (i.e. HD 73882), this band is not visible.

We performed profile fits of the B-X (0,0) and E-X (0,0) bands including all lines of $^{12}C^{16}O$ and $^{13}C^{16}O$ with $J \leq 4$ using the CH component structure. We assumed a $^{12}C^{16}O$ to $^{13}C^{16}O$ ratio of 70, a uniform rotational excitation temperature (T_{rot}) for all levels, and used line parameters from Zhong, et al. (1997). These fits yielded log N(CO) = 14.4 ± 0.4 cm^{-2} and T_{rot} = 3.5 ± 1.3 K. The velocity shift between the models and the spectra only differed from the shift derived from

the H_2 fits in this region by $\sim$0.5 km s^{-1}, implying that most or all of the CO is co-spatial with those molecules.

The CH component structure may not accurately represent the CO component structure, similar to the situation for the HD molecule described earlier in this section. In fact, fits with a variable *b*-value did suggest a smaller velocity dispersion and somewhat larger column density. An extreme case would be if all the CO lies within a single velocity component. Thus, we performed fits assuming that the stronger CH component contains all the CO. In this case, we derive log N(CO) = 15.0 $\pm$ 0.5 cm^{-2}.

The measurements of the A-X bands given by Codina, et al. (1984) were based on a single *IUE* integration. As with our H I measurement, we have co-added the available *IUE* spectrum to improve the S/N. This co-added spectrum allows us to much more precisely measure the equivalent widths of the A-X bands, and these measurements, along with 1-σ uncertaintines, are given in Table 8. With the 2-component CH model, we derive log N(CO) = 14.35 $\pm$ 0.15 cm^{-2}. Despite our use of smaller f-values (Morton & Noreau 1994), in several cases our equivalent widths were considerable smaller than derived by Codina, et al. (1984), and thus our column density is smaller than given by those authors. As with our profile fits, we also performed a curve-of-growth analysis assuming that only the stronger CH component contains CO, and this analysis yields log N(CO) = 14.70 $\pm$ 0.20 cm^{-2}.

Despite nearly identical values of N(H_2), N(CO) for HD 110432 is considerable smaller than for ζ Oph. The latter value was derived from high-resolution, high S/N spectra of the A–X bands with *HST* (Lambert et al. 1994), and is a more precise measurement. However, even our less certain value for HD 110432 is clearly smaller than that for ζ Oph assuming the CH structure toward the former star. Given the other similarities between the two lines of sight, this difference may indicate that indeed nearly all the CO lies within a single velocity component, supporting the larger set of column densities we derived.

The column density of the CH radical has been shown to correlate well with N(H_2) in diffuse clouds (Danks, Federman, & Lambert 1984) and the data point for HD 110432 falls very near the best-fit relationship. Interestingly, an extrapolation of this relationship into the realm of the translucent clouds provides an excellent match for HD 73882 as well.

6. Summary

We have presented the first measurements of far-UV lines of molecular hydrogen for the line of sight toward HD 110432 (A_V = 1.32). We derive a total H_2 column density of log N(H_2) = 20.68 $\pm$ 0.05 cm^{-2}. Combined with log N(H I) = 20.85 $\pm$ 0.15 cm^{-2}, we derive a molecular fraction for hydrogen of $f_{H2} = 0.58 \pm 0.12$. This value is similar to that found for the diffuse cloud line of sight toward ζ Oph and the translucent cloud line of sight toward HD 73882. We find an H_2 kinetic temperature of $T_{kin} = 63 \pm 6$ K. This temperature is in agreement with those found for diffuse

and translucent cloud lines of sight with log N(H_2) $\gtrsim$ 20.5 cm^{-2}.

The excitation of the high-J levels cannot be well-represented by a single temperature model. A two-component model, with $T_{13} = 110 \pm 5$ K, and $T_{35} = 240 \pm 40$ K can account for the data, but does not necessarily have a physical significance. The even-J (para-hydrogen) column densities appear slightly enhanced relative to the odd-J (ortho-hydrogen) column densities. The column densities in each of the rotational states are statistically identical to those from ζ Oph.

Preliminary chemical modeling of the line of sight toward HD 110432 indicates that physical conditions are quite similar to that in the cloud(s) toward ζ Oph. We derive an incident radiation field of about twice the interstellar average, and a density of $\sim$200 cm^{-3}.

The *FUSE* spectra allow us to investigate the diatomic molecules HD and CO. We obtain N(HD) = $15.2^{+0.7}_{-0.4}$ cm^{-2} from a curve-of-growth analysis of 8 $J = 0$ lines, yielding an HD/H_2 ratio of 3×10^{-6}. This lies between that found for ζ Oph and HD 73882, and is much smaller than the value implied by the D/H ratio, suggesting that most deuterium exists outside of HD molecules in the cloud(s) toward HD 110432. However, if HD and CO follow component structures with smaller b-values than H_2, the column densities could be an order of magnitude larger. In particular, profile fits of the HD lines suggest smaller b-values as compared with H_2, and a column density log N(HD) = $16.0^{+0.2}_{-0.3}$ cm^{-2}. The stronger of the two HD components then gives an HD/H_2 ratio very similar to 2×D/H. Based on both a curve-of-growth analysis and profile fitting, we find log N(CO) $\approx$ 14.3 cm^{-2} if CO follows the same component structure at CH, and log N(CO) $\approx$ 14.8 cm^{-2} if all the CO is co-spatial with the stronger of the two CH components.

Overall, in terms of H_2, H I, carbon-containing molecules, and physical conditions, the line of sight toward HD 110432 appears very similar to that of ζ Oph, which has slightly less visual extinction. On the other hand, it does not closely resemble the line of sight toward HD 73882, whose much greater extinction and molecular abundances places it firmly within the realm of translucent clouds. However, preliminary measurements of *FUSE* observations of other translucent cloud lines of sight suggest that the HD 73882 line of sight may not be representative. Many questions regarding the nature of diffuse and translucent clouds may be answered in upcoming studies of such environments with *FUSE*.

This work is based on data obtained for the Guaranteed Time Team by the NASA-CNES-CSA *FUSE* mission operated by the Johns Hopkins University. Financial support to U.S. participants has been provided by NASA contract NAS5-32985. The referee provided much helpful criticism. We also thank W. Blair for helpful comments. This research has made use of the SIMBAD database, operated at CDS, Strasbourg, France.

REFERENCES

Abgrall, H., Roueff, E., & Drira, I., 2000, A&AS, 141, 297

Bakes, E. L. O. & Tielens, A. G. G. M., 1994, ApJ, 427, 822

Black, J. H., & Dalgarno, A. 1973, ApJ, L101

Bohlin, R. C., 1975, ApJ, 200, 402

Codina, S. J., de Freitas Pacheco, J. A., Lopes, D. F., & Gilra, D. 1984, A&AS, 57, 239

Crawford, I. A. 1991, A&A, 246, 210

Crawford, I. A. 1995, MNRAS, 227, 458

Dachs, J., Engels, D., & Kiehling, R. 1988, A&A, 194, 167

Danks, A. C., Federman, S. R., & Lambert, D. L., 1984, A&A, 130, 62

Draine, B. T. 1978, ApJS, 36, 595

ESA, 1997, The Hipparcos and Tycho Catalogues, ESA SP-1200

Falgarone, E., Pineau des Forêts, G., Roueff, E. 1995, A&A, 300, 870

Federman, S. R., Cardelli, J. A., van Dishoeck, E. F., Lambert, D. L., & Black, J. H. 1995, ApJ, 445, 325

Federman, S. R., Weber, J., & Lambert D. L. 1996, ApJ, 463, 181

Ferlet, R., et al. 2000, ApJ, 538, L69

Franco, G. A. P. 1989, A&A, 215, 119

Gredel, R., van Dishoeck, E. F., & Black, J. H. 1993, A&A, 269, 477

Gredel, R., van Dishoeck, E. F., & Black, J. H. 1994, A&A, 285, 300

Hollenbach, D. & Tielens, A. G. G. M. 1999, Rev. Mod. Phys. 71, 173

Joulain, K., Falgarone, E., Pineau des Forêts, G., Flower D. 1998, A&A, 340, 241

Jura, M. 1975, ApJ, 197, 581

Kurucz, R. 1979, ApJS, 40, 1

Lambert, D. L., Sheffer, Y., Gilliland, R. L., & Federman, S. R. 1994, ApJ, 420, 756

Le Bourlot, J., Pineau des Forêts, G., Roueff, E., Flower, D. 1993, A&A, 267, 233

Le Bourlot, J., Pineau des Forêts, G., Roueff, E., Flower, D. 1995, A&A, 302, 870

Le Bourlot, J. 2000, A&A, 360, 656

Mathis, J. S., Mezger, P. G., & Panagis, N. 1983, A&A, 128, 212

Meyer, D. M. & Savage, B. D. 1981, ApJ, 248, 545

Moos, H. W., et al. 2000, ApJ, 538, L1

Morton, D. C. 1975, ApJ, 197, 85

Morton, D. C. & Noreau, L. 1994, ApJS, 95, 301

Nyman, L.-Å., Bronfman, L., & Thaddeus, P. 1989, A&A, 216, 185

Pineau des Forêts, G., Flower, D. R., Hartquist, T. W., Dalgarno, A. 1986, MNRAS, 220, 801

Rodgers, A. W. 1960, MNRAS, 120, 163

Roueff, E., Abgrall, H., Liu, X.M., & Shemanskii, D. 2000, H_2 in Space, (Cambridge: Cambridge University Press), ed. F. Combes and G. Pineau des Forêts, 13

Savage, B. D., Drake, J. F., Budich, W., & Bohlin, R. C. 1977, ApJ, 216, 291

Savage, B. D. & Sembach K. R. 1996, ARA&A, 34, 279

Seidensticker, K. J. 1989, A&AS, 79, 61

Seidensticker, K. J. & Schmidt-Kaler, T. 1989, A&A, 225, 192

Serkowski, K., Mathewson, D. L., & Ford, V. L. 1975, ApJ, 196, 261

Snow, T. P. 1993, ApJ, 402, L73

Snow, T. P., et al. 2000, ApJ, 538, L65

Spitzer, L. & Cochran, W. D. 1973, L23

van Dishoeck, E. F. & Black, J. H. 1986, ApJ, 307, 332

van Dishoeck, E. F., & Black, J. H. 1989, ApJ, 340, 273

Whittet, D. C. B. & van Breda, I. G. 1978, A&A, 66, 57

Zhong, Z. P, Feng, R. F., Xu, S. L., Wu, S. L., Zhu, L. F., Zhang, X. J., Ji, Q. & Shi, Q. C. 1997, Phys. Rev. A, 55, 1799

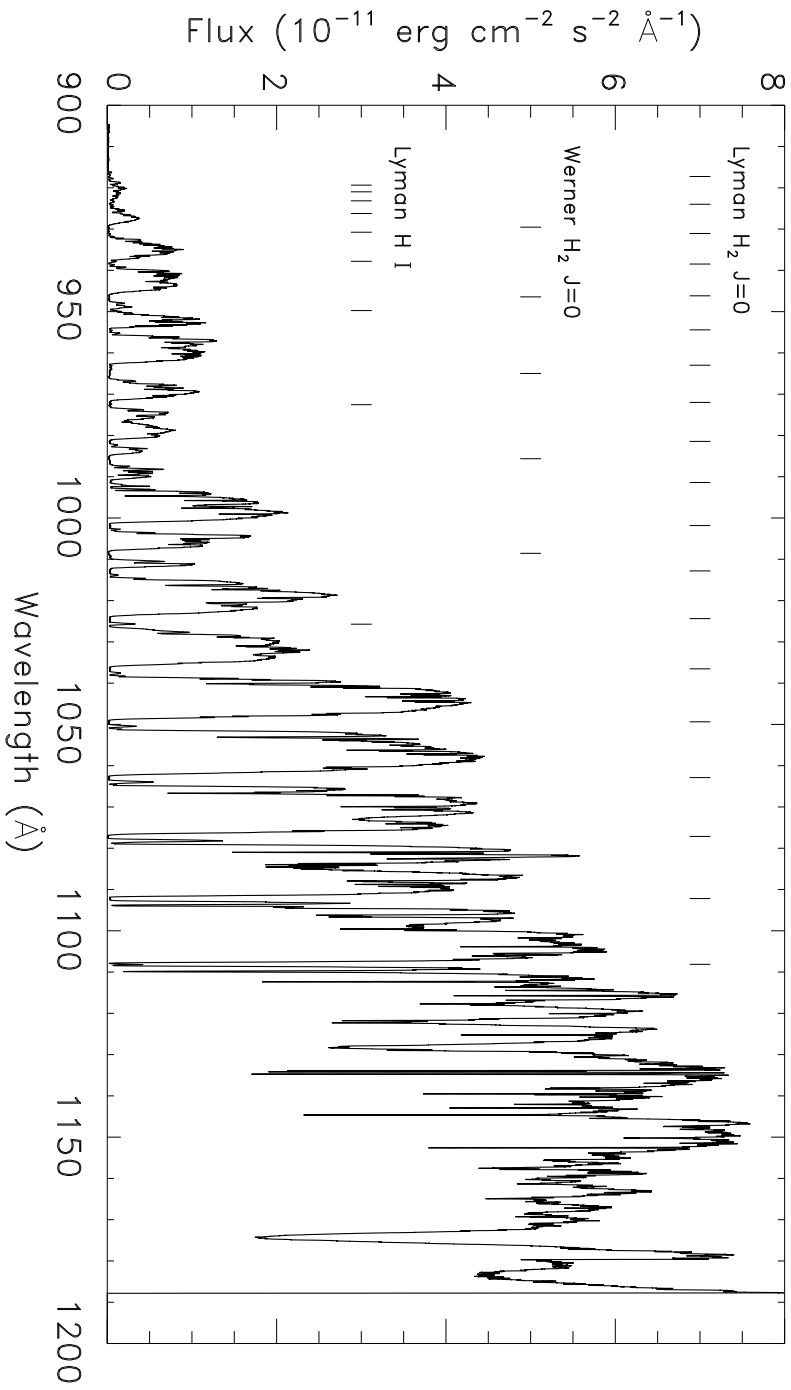

Fig. 1.— Total merged spectrum for HD 110432 from all detector segments and all exposures. Lyman series H_2 bandheads for the (18,0) through (0,0) vibrational bands are indicated by the top set of tickmarks. The middle set depicts the bandheads for the Werner series of H_2 for the (4,0) through (0,0) bands. The bottom set marks Lyman series H I lines from N=10 through β.

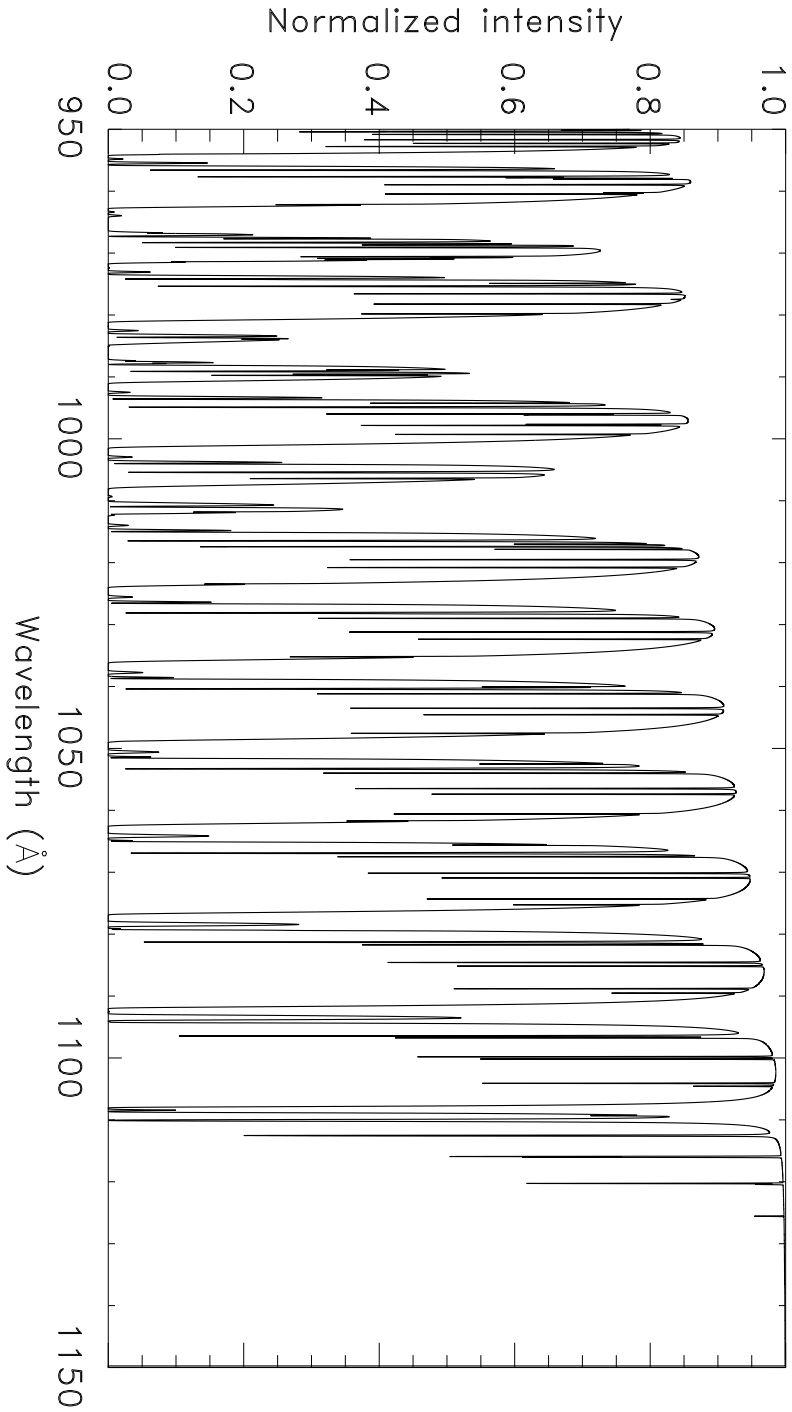

Fig. 2.— Normalized H_2 model spectrum for HD 110432 based on our derived rotational populations. Note particularly that the high points between vibrational bands do not reach the continuum. We only fitted vibrational bands at the longer wavelengths where this problem is minimized. This model does not include H I lines which become a progressively larger problem for shorter wavelengths, nor the stellar continuum and the effects of extinction apparent in Figure 1.

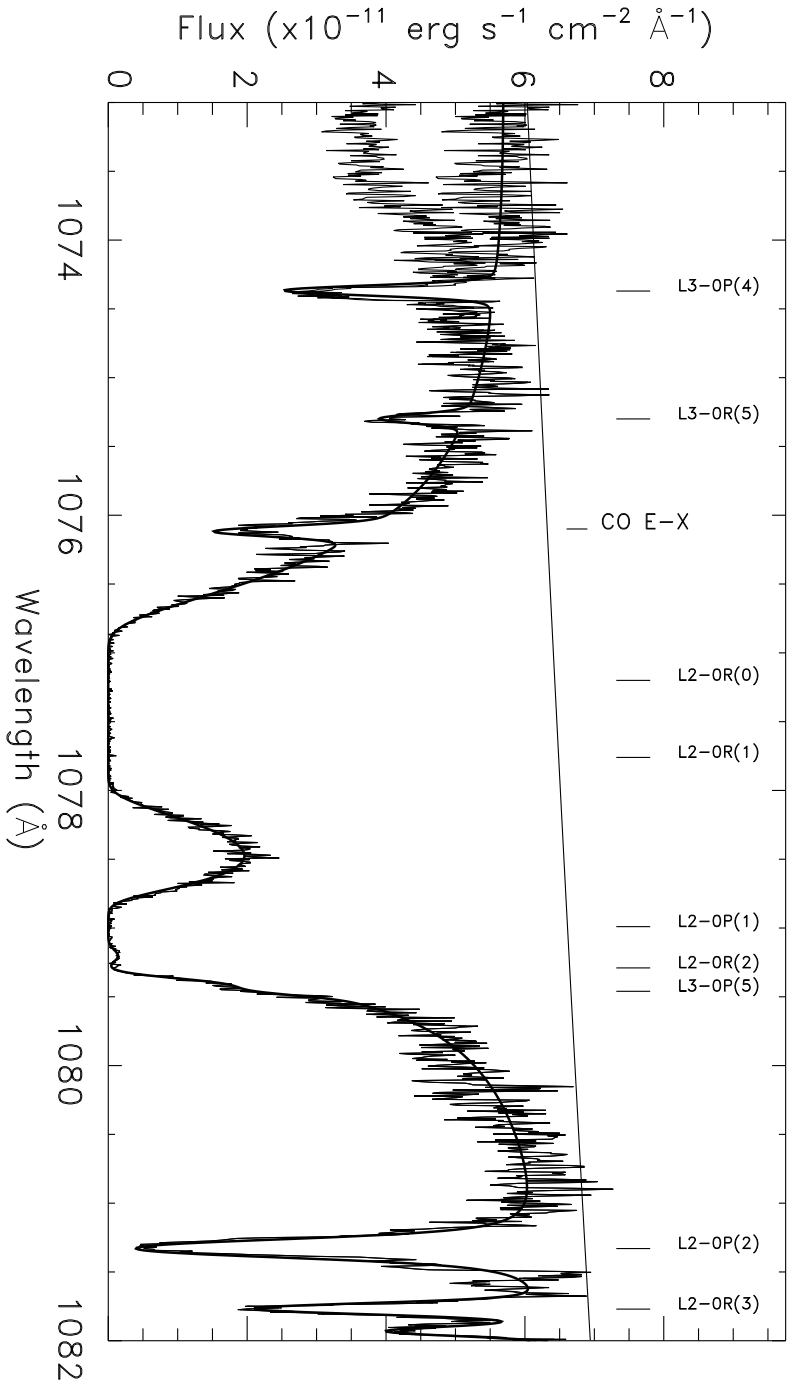

Fig. 3.— H_2 profile fit for the Lyman (2,0) band from SiC 2B. The line above the spectrum (actually slightly curved) depicts the continuum derived in the fit. A stellar feature at 1073 Å was removed and the plot shows both the original and corrected spectra. For computational simplicity, we modeled the CO E–X (0,0) band as a single line. While this gives a less-than-optimal fit for the line itself, it does not affect the overall fit for the J=0–2 lines. The CO column density quoted in § 5 is not based on this simplified model.

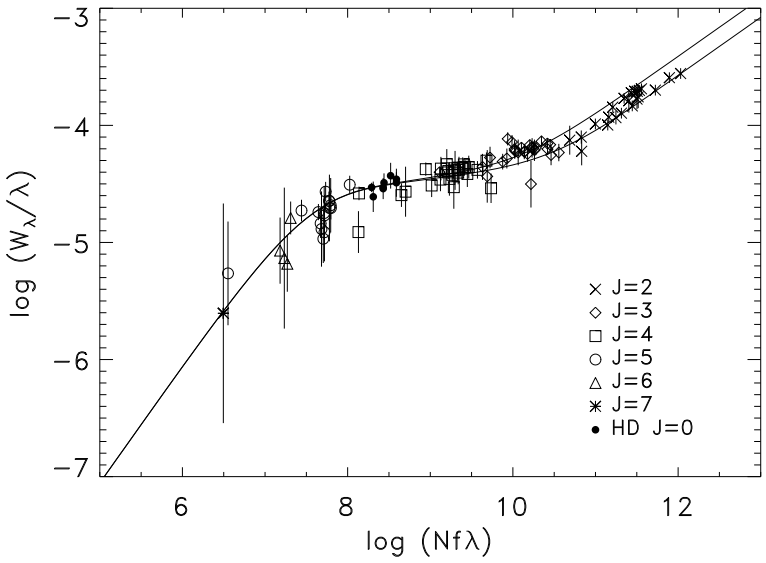

Fig. 4.— Two-component curve of growth for HD 110432. The two curves represent the range in damping constants for the measured lines.

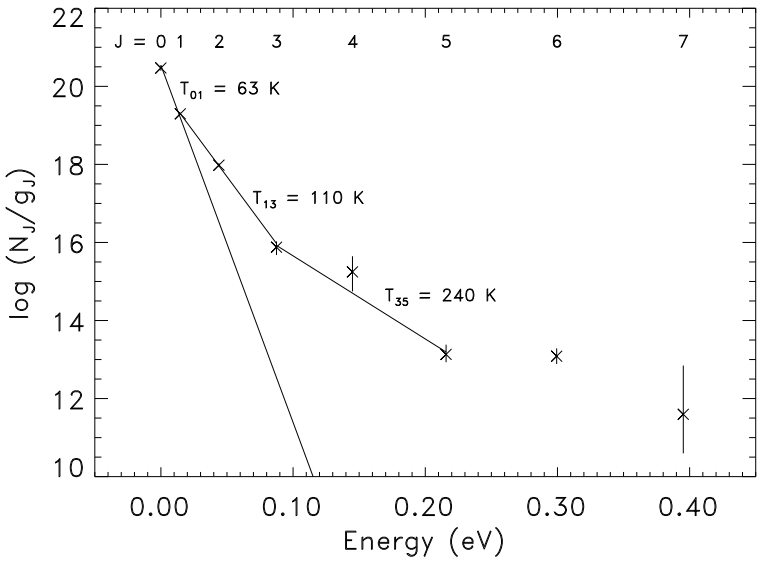

Fig. 5.— Excitation diagram for HD 110432. The solid lines correspond to linear fits to $J = 0$–1, $J = 1$–3, and $J = 3$–5, as described in the text.

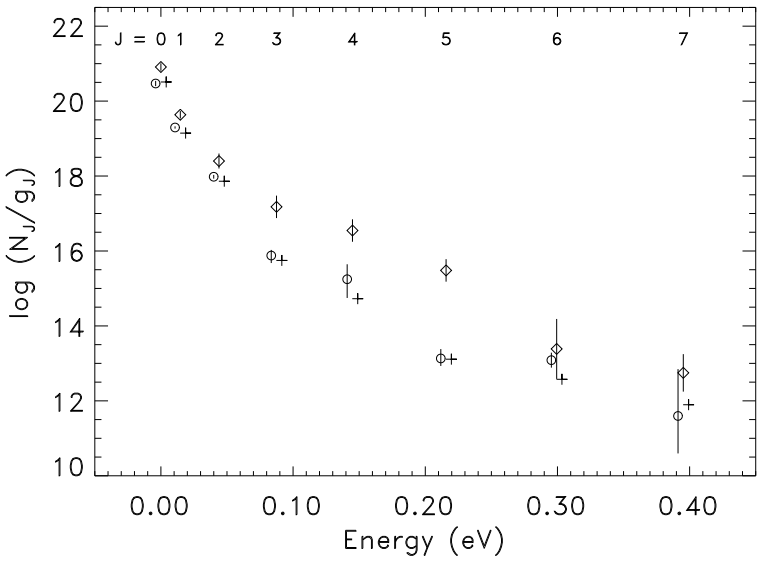

Fig. 6.— Comparison of H_2 excitation in three lines of sight. Symbols used: HD 110432 - circles; HD 73882 - diamonds, ζ Oph - crosses. Error bars are not given for ζ Oph. Data points have been slightly offset horizontally to separate the three datasets.

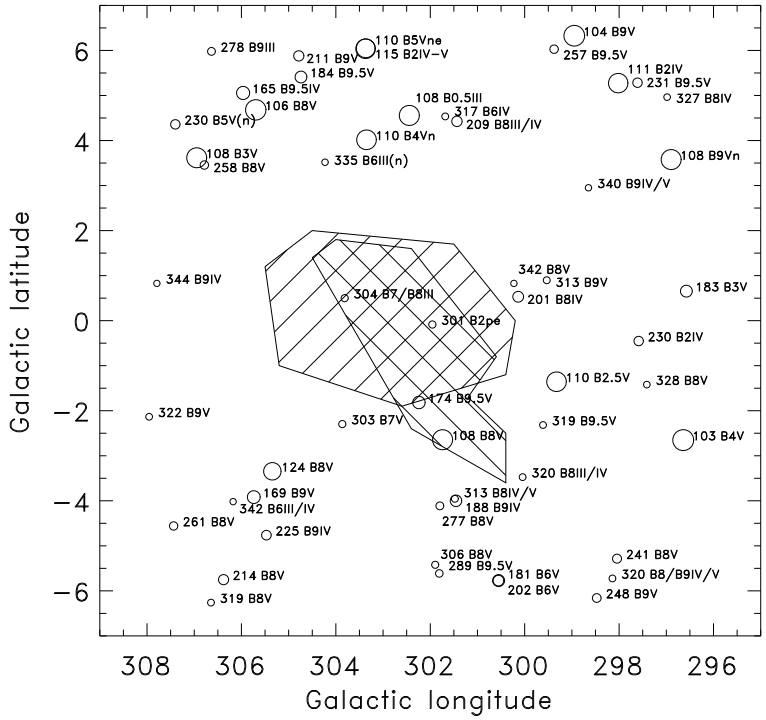

Fig. 7.— Early-type stars near the HD 110432 line of sight. The symbol size is inversely proportional to the *Hipparcos* distance. This distance in parsecs is given to the right of the star, along with the spectral type. Only stars between 100 and 350 pc were included. HD 110432 itself lies at the center of the plot. An approximate depiction of the two-cloud structure of the Coalsack from Seidensticker & Schmidt-Kaler (1989) is given by the hatched areas. The more distant cloud extends to more negative latitudes. The scale of the plot at the distance of the nearer cloud is about 3 pc per degree.

Table 1. Adopted H_2 component structure

Comp.	Rel. strength	b (km s^{-1})	$v_{\rm helio}$[a] (km s^{-1})
1	0.324	1.8	+ 2.9
2	0.676	1.4	+ 6.9

[a]Subtract 7.6 km s^{-1} to obtain $v_{\rm LSR}$

Table 2. Previous absorption-line abundance data for HD 110432

Species	log N (cm^{-2})	Reference
K I	11.86	Crawford 1995
Ca II	11.97	Crawford 1995
CH	13.19	Crawford 1995
CH^+	13.25	Crawford 1995
CN	12.08	Gredel et al. 1993
C_2	13.48	van Dishoeck & Black 1989
CO	14.60	Codina et al. 1984

Table 3. Band-by-band fits

Detector segment	Band	log N(0) (cm^{-2})	log N(1) (cm^{-2})	log N(2) (cm^{-2})
LiF 1A	(4,0)	20.44	20.26	18.68
LiF 2B	(4,0)	20.39	20.28	18.67
SiC 1A	(4,0)	20.43	20.28	18.67
SiC 2B	(4,0)	20.40	20.27	18.66
Mean	(4,0)	20.42	20.27	18.67
LiF 1A	(3,0)	20.57	20.29	18.72
LiF 2B	(3,0)	20.56	20.27	18.74
SiC 1A	(3,0)	20.59	20.25	18.73
SiC 2B	(3,0)	20.55	20.24	18.71
Mean	(3,0)	20.57	20.26	18.73
LiF 1A	(2,0)	20.44	20.21	18.59
SiC 1A	(2,0)	20.40	20.25	18.71
SiC 2B	(2,0)	20.42	20.24	18.60
Mean	(2,0)	20.42	20.23	18.63
LiF 2A	(1,0)	20.49	20.24	18.68
SiC 2B	(1,0)	20.45	20.21	18.64
Mean	(1,0)	20.47	20.23	18.66
Mean	All	20.47	20.25	18.68

Table 4. Rotational populations for H_2 and HD

Species	J	log N_J (cm^{-2})
H_2	0	20.47 ± 0.07
...	1	20.25 ± 0.03
...	2	18.68 ± 0.05
...	3	$17.20^{+0.15}_{-0.20}$
...	4	$16.20^{+0.40}_{-0.50}$
...	5	$14.65^{+0.25}_{-0.20}$
...	6	$14.20^{+0.20}_{-0.20}$
...	7	$13.25^{+1.25}_{-1.00}$
...	Total	20.68 ± 0.06
HD[a]	0	$15.20^{+0.70}_{-0.40}$

[a]Curve of growth value; see text for information on profile fits.

Table 5. Line of sight properties comparison

Line of sight	$E(B-V)$	A_V	R_V	T_{kin} (K)	log N(H_2) (cm^{-2})	log N(H I) (cm^{-2})	f_{H2}
Zeta Oph	0.32	0.99	3.1	54	20.65	20.72	0.63
HD 110432	0.40	1.32	3.3	63	20.68	20.85	0.58
HD 73882	0.72	2.44	3.4	59	21.08	21.11	0.65

Table 6. Modeled column densities

Model	n_H (cm^{-3})	G_0	r_{min} (cm)	T (K)	log N(H I) (cm^{-2})	log N(H_2) (cm^{-2})	log N(HD) (cm^{-2})	log N(CH) (cm^{-2})
A	100	1	1×10^{-6}	70	20.65	20.74	16.17	12.89
B	100	1	3×10^{-6}	61	20.81	20.70	16.28	12.81
C	200	2	3×10^{-6}	65	20.79	20.72	16.04	12.84
D	500	5	3×10^{-6}	76	20.79	20.72	15.08	12.84

Table 7. Observed vs. modeled H_2 high-J excitation

	log N(J)				
J	Obs.	Model A	Model B	Model C	Model D
0	20.47	20.50	20.49	20.45	20.46
1	20.25	20.44	20.28	20.31	20.42
2	18.68	18.10	17.48	17.78	18.30
3	17.20	16.57	15.47	15.76	16.21
4	16.20	14.40	14.34	14.62	15.01
5	14.65	13.99	13.89	14.18	14.60
6	14.20	13.01	12.92	13.22	13.63
7	13.25	12.95	12.90	13.18	13.59

Table 8. CO A-X band measurements

Band	λ (Å)	W_λ (mÅ)
(1-0)	1509.76	76.4 ± 7.3
(2-0)	1477.54	79.0 ± 16.4
(3-0)	1447.34	72.0 ± 16.3
(4-0)	1419.03	65.5 ± 24.6
(6-0)	1367.62	30.6 ± 28.1
(7-0)	1344.18	24.2 ± 13.5